
Scattering GCN: Overcoming Oversmoothness in Graph Convolutional Networks

Yimeng Min^{*1} Frederik Wenkel^{*21} Guy Wolf²¹

Abstract

Graph convolutional networks (GCNs) have shown promising results in processing graph data by extracting structure-aware features. This gave rise to extensive work in geometric deep learning, focusing on designing network architectures that ensure neuron activations conform to regularity patterns within the input graph. However, in most cases the graph structure is only accounted for by considering the similarity of activations between adjacent nodes, which in turn degrades the results. In this work, we augment GCN models by incorporating richer notions of regularity by leveraging cascades of band-pass filters, known as geometric scatterings. The produced graph features incorporate multiscale representations of local graph structures, while avoiding overly smooth activations forced by previous architectures. Moreover, inspired by skip connections used in residual networks, we introduce graph residual convolutions that reduce high-frequency noise caused by joining together information at multiple scales. Our hybrid architecture introduces a new model for semi-supervised learning on graph-structured data, and its potential is demonstrated for node classification tasks on multiple graph datasets, where it outperforms leading GCN models.

1. Introduction

Deep learning approaches are at the forefront of modern machine learning. While they are effective in a multitude of applications, their most impressive results are typically achieved when processing data with inherent structure that can be used to inform the network architecture or the neu-

ron connectivity design. For example, image processing tasks gave rise to convolutional neural networks that rely on spatial organization of pixels, while time-series analysis gave rise to recurrent neural networks that leverage temporal organization in their information processing via feedback loops and memory mechanisms. The success of neural networks in such applications, traditionally associated with signal processing, has motivated the emergence of geometric deep learning, with the goal of generalizing the design of structure-aware network architectures from Euclidean spatiotemporal structures to a wide range of non-Euclidean geometries that often underlie modern data.

Geometric deep learning approaches typically use graphs as a model for data geometries, either by constructing them from input data (e.g., via similarity kernels) or directly given as quantified interactions between data points (Bronstein et al., 2017). Using such models, recent works have shown that graph neural networks (GNNs) perform well in multiple application fields, including biology, chemistry and social networks (Gilmer et al., 2017; Hamilton et al., 2017; Kipf & Welling, 2016). It should be noted that most GNNs consider each graph together with given node features, as a generalization of images or audio signals, and thus aim to compute whole-graph representations. These, in turn, can be applied to graph classification, for example when each graph represents the molecular structure of proteins or enzymes classified by their chemical properties (Fout et al., 2017; De Cao & Kipf, 2018; Knyazev et al., 2018).

On the other hand, methods such as graph convolutional networks (GCNs) presented by Kipf & Welling (2016) consider node-level tasks and in particular node classification. As explained in Kipf & Welling (2016), such tasks are often considered in the context of semi-supervised learning, as typically only a small portion of nodes on the graph possess labels. In these settings, the entire dataset is considered as one graph and the network is tasked with learning node representations that infer information from node features as well as the graph structure. However, most state-of-the-art approaches for incorporating graph structure information in neuronal network operations aim to enforce similarity between representations of adjacent (or neighboring) nodes, which essentially implements local smoothing of neuron activations over the graph (Li et al., 2018). While such

^{*}Equal contribution ¹Mila – Quebec AI Institute, Montréal, QC, Canada ²Department of Mathematics & Statistics, Université de Montréal, Montréal, QC, Canada. Correspondence to: Yimeng Min <yimeng.min@mail.utoronto.ca>, Guy Wolf <guy.wolf@umontreal.ca>.

smoothing operations may be sufficiently effective in whole-graph settings, they often cause degradation of results in semi-supervised node processing tasks due to oversmoothing (NT & Maehara, 2019; Li et al., 2018), as nodes become indistinguishable with deeper and increasingly complex network architectures.

In this work, we focus on the above mentioned node-level processing and aim to tackle the oversmoothing problem by introducing neural pathways that encode higher-order forms of regularity in graphs. Our construction is inspired by recently proposed scattering networks on graphs (Gama et al., 2018; Gao et al., 2019; Zou & Lerman, 2019), which have proven to be effective for whole-graph representation and classification. These networks generalize the Euclidean scattering transform, which was originally presented by Mallat (2012) as a mathematical model for convolutional neural networks. In graph settings, the scattering construction leverages deep cascades of graph wavelets (Hammond et al., 2011; Coifman & Maggioni, 2006) and pointwise nonlinearities to capture multiple modes of variations from graph features or labels. Using the terminology of graph signal processing, these can be considered as generalized band-pass filtering operations, while GCNs (and many other GNNs) can be considered as relying on low-pass filters. Here, we propose to combine together the strengths of GCNs on node-level tasks together with the ones indicated by scattering networks on whole-graph tasks.

The paper is structured as follows. Sec. 1.1 and 1.2 discuss related works and the notations used in this paper. Sec. 2 provides preliminaries on graph signal processing. Sec. 3 and 4 discuss the GCN approach and geometric scattering models to briefly unify their formulation to be consistent with this work. Then, Sec. 5 and 6 present our new architecture components combining ideas from these two models. Finally, Sec. 7 provides empirical results followed by our conclusions in Sec. 8.

1.1. Related Work

As many applied fields such as Bioinformatics and Neuroscience heavily rely on the analysis of graph-structured data, the study of reliable classification methods has received much attention lately. In this work, we focus on the particular class of semi-supervised classification tasks, where Kipf & Welling (2016); Li et al. (2018) had success using GCN models. Their theoretical study reveals that graph convolutions can be interpreted as Laplacian smoothing operations, which poses fundamental limitations on the approach. Further, NT & Maehara (2019) developed a theoretical framework based on graph signal processing, relying on the relation between frequency and feature noise, to show that GNNs perform a low-pass filtering on the feature vectors. In Abu-El-Haija et al. (2019) multiple powers of

the adjacency matrix were used to learn the higher-order neighborhood information, while Liao et al. (2019) used Lanczos algorithm to construct a low-rank approximation of the graph Laplacian that efficiently gathers the multiscale information, demonstrated on citation networks and the QM8 quantum chemistry dataset. Finally, Xu et al. (2019) studied wavelets on graphs and collected higher-order neighborhood information based on wavelet transformation.

Together with the study of learned networks, recent studies have also introduced the construction of geometric scattering transforms, relying on manually crafted families of graph wavelet transforms (Gama et al., 2018; Gao et al., 2019; Zou & Lerman, 2019). Similar to the initial motivation of geometric deep learning to generalize convolutional neural networks, the geometric scattering framework generalizes the construction of Euclidean scattering from Mallat (2012) to the graph setting. Theoretical studies (e.g., Gama et al., 2018; 2019) established the stability of these generalized scattering transforms to perturbations and deformations of graphs and signals on them. Moreover, the practical application of geometric scattering to whole-graph data analysis was studied in Gao et al. (2019), achieving strong classification results on social networks and biochemistry data, which established the effectiveness of this approach.

In this work, we aim to combine the complementary strengths of GCN models and geometric scattering, and to provide a new avenue for incorporating richer notions of regularity into GNNs. Furthermore, our construction integrates trained task-driven components in geometric scattering architectures. Finally, while most previous work on geometric scattering focused on whole-graph settings, we consider node-level processing which requires new considerations about the construction.

1.2. Notation

We denote matrices and vectors with bold letters with uppercase letters representing matrices and lowercase letters representing vectors. In particular, $\mathbf{I}_n \in \mathbb{R}^{n \times n}$ is used for the identity matrix and $\mathbf{1}_n \in \mathbb{R}^n$ denotes the vector with ones in every component. We write $\langle \cdot, \cdot \rangle$ for the standard scalar product in \mathbb{R}^n . We will interchangeably consider functions of graph nodes as vectors indexed by the nodes, implicitly assuming a correspondence between a node and a specific index. This carries over to matrices, where we relate nodes to column or row indices. We further use the abbreviation $[n] := \{1, \dots, n\}$ where $n \in \mathbb{N}$.

2. Graph Signal Processing

Let $G = (V, E, w)$ be a weighted graph where $V := \{v_1, \dots, v_n\}$ is the set of nodes, $E \subset \{\{v_i, v_j\} \in V \times V, i \neq j\}$ is the set of (undirected) edges and $w : E \rightarrow$

$(0, \infty)$ assigns (positive) edge weights to the graph edges. We note that w can equivalently be considered as a function of $V \times V$, where we set the weights of non-adjacent node pairs to zero. We define a *graph signal* as a function $x : V \rightarrow \mathbb{R}$ on the nodes of G and aggregate them in a signal vector $\mathbf{x} \in \mathbb{R}^n$ with the i^{th} entry being $x(v_i)$.

We define the (combinatorial) *graph Laplacian* matrix $\mathbf{L} := \mathbf{D} - \mathbf{W}$, where $\mathbf{W} \in \mathbb{R}^{n \times n}$ is the *weighted adjacency matrix* of the graph G given by

$$\mathbf{W}[v_i, v_j] := \begin{cases} w(v_i, v_j) & \text{if } \{v_i, v_j\} \in E \\ 0 & \text{otherwise} \end{cases},$$

and $\mathbf{D} \in \mathbb{R}^{n \times n}$ is the *degree matrix* of G defined by $\mathbf{D} := \text{diag}(d_1, \dots, d_n)$ with $d_i := \text{deg}(v_i) := \sum_{j=1}^n \mathbf{W}[v_i, v_j]$ being the *degree* of the node v_i .

In practice, we work with the (symmetric) *normalized Laplacian* matrix

$$\mathcal{L} := \mathbf{D}^{-1/2} \mathbf{L} \mathbf{D}^{-1/2} = \mathbf{I}_n - \mathbf{D}^{-1/2} \mathbf{W} \mathbf{D}^{-1/2}.$$

Conveniently, \mathcal{L} has the property of being symmetric positive semi-definite, and thus being orthogonally diagonalizable according to

$$\mathcal{L} = \mathbf{Q} \mathbf{\Lambda} \mathbf{Q}^T = \sum_{i=1}^n \lambda_i \mathbf{q}_i \mathbf{q}_i^T,$$

where $\mathbf{\Lambda} := \text{diag}(\lambda_1, \dots, \lambda_n)$ is the diagonal matrix with the eigenvalues on the main diagonal and \mathbf{Q} is the orthogonal matrix containing the corresponding normalized eigenvectors $\mathbf{q}_1, \dots, \mathbf{q}_n \in \mathbb{R}^n$ as its columns. This can be seen by writing

$$\mathcal{L} = \sum_{v \sim w} w(v, w) \mathbf{D}^{-1/2} \mathbf{B}_{v,w} \mathbf{D}^{-1/2},$$

where $\mathbf{B}_{v,w} \in \mathbb{R}^{n \times n}$, $\mathbf{B}_{v,w}[v, v] = \mathbf{B}_{v,w}[w, w] = 1$, $\mathbf{B}_{v,w}[v, w] = \mathbf{B}_{v,w}[w, v] = -1$ and all remaining values being zero. Expanding the inner product $\mathbf{x}^T \mathcal{L} \mathbf{x}$ according to this formulation establishes positive semi-definiteness of \mathcal{L} because the weights are strictly positive and $\tilde{\mathbf{x}}^T \mathbf{B}_{v,w} \tilde{\mathbf{x}} = (\tilde{\mathbf{x}}[v] - \tilde{\mathbf{x}}[w])^2 \geq 0$ where $\tilde{\mathbf{x}} := \mathbf{D}^{-1/2} \mathbf{x}$.

A detailed study of the eigenvalues reveals that

$$0 = \lambda_1 \leq \lambda_2 \leq \dots \leq \lambda_n \leq 2.$$

The lower bound is easily verified by recalling that positive semi-definite matrices only exhibit non-negative eigenvalues followed by checking that $\mathbf{q}_1 := \mathbf{D}^{1/2} \mathbf{1}_n$ is an eigenvector corresponding to $\lambda_1 = 0$. The upper bound has been established for example in Chung (1997).

We can interpret the $\lambda_i, i \in [n]$ as the frequency magnitudes and \mathbf{q}_i as the corresponding harmonics. We accordingly

define the *Fourier transform* of a signal vector $\mathbf{x} \in \mathbb{R}^n$ by $\hat{\mathbf{x}}[i] = \langle \mathbf{x}, \mathbf{q}_i \rangle$ for $i \in [n]$. The corresponding inverse Fourier transform is given by $\mathbf{x} = \sum_{i=1}^n \hat{\mathbf{x}}[i] \mathbf{q}_i$. Note that this can be written compactly as

$$\hat{\mathbf{x}} = \mathbf{Q}^T \mathbf{x}, \quad \mathbf{x} = \mathbf{Q} \hat{\mathbf{x}}.$$

Finally, we introduce the concept of *graph convolutions*. We define a filter $g : V \rightarrow \mathbb{R}$ defined on the set of nodes and want to convolve the corresponding filter vector $\mathbf{g} \in \mathbb{R}^n$ with a signal vector $\mathbf{x} \in \mathbb{R}^n$, i.e. $\mathbf{g} \star \mathbf{x}$. To explicitly compute this convolution, we recall that in the Euclidean setting, the convolution of two signals equals the product of their corresponding frequencies. This property generalizes to graphs (Shuman et al., 2013) in the sense that $(\widehat{\mathbf{g} \star \mathbf{x}})[i] = \hat{\mathbf{g}}[i] \hat{\mathbf{x}}[i]$ for $i \in [n]$. Applying the inverse Fourier transform yields

$$\begin{aligned} \mathbf{g} \star \mathbf{x} &= \sum_{i=1}^n \hat{\mathbf{g}}[i] \hat{\mathbf{x}}[i] \mathbf{q}_i \\ &= \sum_{i=1}^n \hat{\mathbf{g}}[i] \langle \mathbf{q}_i, \mathbf{x} \rangle \mathbf{q}_i = \mathbf{Q} \widehat{\mathbf{G}} \mathbf{Q}^T \mathbf{x}, \end{aligned}$$

where $\widehat{\mathbf{G}} := \text{diag}(\hat{\mathbf{g}}) = \text{diag}(\hat{\mathbf{g}}[1], \dots, \hat{\mathbf{g}}[n])$. Therefore, we can parametrize the convolution with a filter by directly considering the Fourier coefficients in $\widehat{\mathbf{G}}$.

Furthermore, it can be verified (Defferrard et al., 2016) that when these coefficients are defined as polynomials $\hat{\mathbf{g}}[i] := \sum_k \gamma_k \lambda_i^k$ for $i \in \mathbb{N}$ of the Laplacian eigenvalues in $\mathbf{\Lambda}$ (i.e. $\widehat{\mathbf{G}} = \sum_k \gamma_k \mathbf{\Lambda}^k$), the resulting filter convolution are localized in space and can be written in terms of \mathcal{L} as

$$\mathbf{g} \star \mathbf{x} = \sum_k \gamma_k \mathcal{L}^k \mathbf{x}$$

without requiring spectral decomposition of the normalized Laplacian. This property motivates the standard practice of using filters that have polynomial forms, which is studied in previous works on graph convolutional networks and geometric scattering as well as this work.

3. Graph Convolutional Network

The initial idea of learning convolutional filters on graphs consists of learning the parameter $\hat{\mathbf{g}}$. This has however two immediate drawbacks as pointed out in Defferrard et al. (2016). The filters cannot be localized in the feature space and their computation is expensive ($\mathcal{O}(n)$). Similar to Kipf & Welling (2016), we are interested in a semi-supervised setting where only a small portion of the nodes is labeled. Their method relies on the construction of a model $f(\mathbf{X}, \mathbf{W})$ that does not only use the labeled data, but also leverages the intrinsic geometric information encoded in the adjacency

matrix \mathbf{W} . This is done by enforcing similarity between adjacent nodes and propagating information from the labeled nodes over the whole set of nodes.

The convolutional filter is parametrized by $\hat{g}[i] := \theta(2 - \lambda_i)$. This parametrization yields

$$\mathbf{g}_\theta \star \mathbf{x} = \theta \left(\mathbf{I}_n + \mathbf{D}^{-1/2} \mathbf{W} \mathbf{D}^{-1/2} \right) \mathbf{x}. \quad (1)$$

The choice of only one learnable parameter θ is made to avoid overfitting. The matrix $\mathbf{I}_n + \mathbf{D}^{-1/2} \mathbf{W} \mathbf{D}^{-1/2}$ has eigenvalues in $[0, 2]$. This could lead to vanishing or exploding gradients. This issue is addressed by the following renormalization trick (Kipf & Welling, 2016): $\mathbf{I}_n + \mathbf{D}^{-1/2} \mathbf{W} \mathbf{D}^{-1/2} \rightarrow \tilde{\mathbf{D}}^{-1/2} \tilde{\mathbf{W}} \tilde{\mathbf{D}}^{-1/2}$, where $\tilde{\mathbf{W}} := \mathbf{I}_n + \mathbf{W}$ and $\tilde{\mathbf{D}} := \sum_{i=1}^n \tilde{\mathbf{W}}_{ij}$. This operation replaces the features of the nodes by a weighted average of itself and its neighbors. Note that the repeated execution of graph convolutions will enforce similarity throughout higher-order neighborhoods with order equal to the number of staggered layers. Setting

$$\mathbf{A} := \tilde{\mathbf{D}}^{-1/2} \tilde{\mathbf{W}} \tilde{\mathbf{D}}^{-1/2},$$

the complete layer-wise propagation rule takes the form

$$\mathbf{h}_j^\ell = \sigma \left(\sum_{i=1}^{N_{\ell-1}} \underbrace{\theta_i^\ell \mathbf{A} \mathbf{h}_i^{\ell-1}}_{\mathbf{g}_{\theta_i^\ell} \star \mathbf{h}_i^{\ell-1}} \right).$$

Here, ℓ indicates the layer with N_ℓ neurons, $\mathbf{h}_j^\ell \in \mathbb{R}^n$ the activation vector of the j^{th} neuron, θ_i^ℓ the learned parameter of the convolution with the i^{th} incoming activation vector from the preceding layer and $\sigma(\cdot)$ an element-wise applied activation function. Written in matrix notation, this gives

$$\mathbf{H}^\ell = \sigma \left(\mathbf{A} \mathbf{H}^{\ell-1} \Theta^\ell \right), \quad (2)$$

where $\Theta^\ell \in \mathbb{R}^{N_{\ell-1} \times N_\ell}$ is the weight-matrix of the ℓ^{th} layer and $\mathbf{H}^\ell \in \mathbb{R}^{n \times N_\ell}$ contains the activations outputted by the ℓ^{th} layer.

We want to remark that the above explained GCN model can be interpreted as a low-pass operation. For the sake of simplicity, let us consider the convolutional operation (1) before the reparametrization trick. If we observe the convolution operation as the summation

$$\mathbf{g}_\theta \star \mathbf{x} = \sum_{i=1}^n \gamma_i \hat{\mathbf{x}}[i] \mathbf{q}_i,$$

we clearly see that higher weights $\gamma_i = \theta(2 - \lambda_i)$ are put on the low-frequency harmonics, while high-frequency harmonics are progressively less involved as $0 = \lambda_1 \leq$

$\lambda_2 \leq \dots \leq \lambda_n \leq 2$. This indicates that the model can only access a diminishing portion of the original information contained in the input signal the more graph convolutions are staggered.

This observation is in line with the well-known oversmoothing problem (Li et al., 2018) related to GCN models. The repeated application of graph convolutions will successively smooth the signals of the graph such that nodes can not be distinguished anymore.

4. Geometric Scattering

In this section, we recall the concept of geometric scatterings on graphs. These are based on the *lazy random walk* matrix

$$\mathbf{P} := \frac{1}{2} (\mathbf{I}_n + \mathbf{W} \mathbf{D}^{-1}),$$

which is closely related to the *graph random walk*, a Markov process with transition matrix $\mathbf{R} := \mathbf{W} \mathbf{D}^{-1}$. The matrix \mathbf{P} however allows self loops while normalizing by a factor of two in order to retain a Markov process.

Therefore, considering a distribution $\mu_0 \in \mathbb{R}^n$ of the initial position of the lazy random walk, its positional distribution after t steps is encoded by $\mu_t = \mathbf{P}^t \mu_0$.

It was shown in Gao et al. (2019) that the propagation of a graph signal vector $\mathbf{x} \in \mathbb{R}^n$ by this Markov operator, i.e. $\mathbf{x}_t = \mathbf{P}^t \mathbf{x}$, is a low-pass operation which preserves the zero-frequencies of the signal while suppressing high frequencies.

This limitation is addressed by introducing the *wavelet* matrix $\Psi_k \in \mathbb{R}^{n \times n}$ of scale 2^k ,

$$\Psi_k := \mathbf{P}^{2^{k-1}} - \mathbf{P}^{2^k} = \mathbf{P}^{2^{k-1}} (\mathbf{I}_n - \mathbf{P}^{2^{k-1}}).$$

This leverages the fact that high frequencies can be recovered with multiscale wavelet transforms as the one which decompose the non-zero frequencies into dyadic frequency bands. The operation $(\Psi_k \mathbf{x})[v_i]$ collects signals from a neighborhood of order 2^k but applies no averaging operation over them.

Geometric scattering was originally introduced in the context of whole-graph classification and consisted of aggregating *scattering features*. These are stacked wavelet transforms parameterized via tuples $J := (k_1, \dots, k_m) \in \cup_{m \in \mathbb{N}} \mathbb{N}^m$ containing the bandwidth scale parameters, which are separated by element-wise absolute value nonlinearities according to

$$\Phi_J \mathbf{x} := \Psi_{k_m} |\Psi_{k_{m-1}} \dots |\Psi_{k_2} |\Psi_{k_1} \mathbf{x} || \dots |, \quad (3)$$

where m corresponds to the length of the tuple J . The scattering features are aggregated over the whole graph by

taking q^{th} -order moments over the set of nodes,

$$S(J, q)\mathbf{x} := \sum_{i=1}^n |\Phi_J \mathbf{x}[v_i]|^q. \quad (4)$$

As our research is devoted to the study of node-based classification we reinvent this approach in a new context, keeping the scattering transforms Φ_J on a node-level by dismissing the aggregation step (4). For each tuple J , we define the following scattering propagation rule, which mirrors the GCN rule but replaces the low-pass filter by a geometric scattering operation resulting in

$$\mathbf{H}^\ell = \sigma \left(\Phi_J \mathbf{H}^{\ell-1} \Theta^\ell \right). \quad (5)$$

We note that in practice we only choose a subset of tuples, which is chosen as part of the network design explained in the following section.

5. Combining GCN and Scattering Models

To combine the benefits of GCN models and geometric scatterings adapted to the node level, we now propose a hybrid network structure as shown in Fig. 1. This structure combines low-pass operations based on the GCN model with band-pass operations based on geometric scattering. We will first introduce the general architecture of the model.

To define the layer-wise propagation rule, we introduce

$$\mathbf{H}_{gcn}^\ell := \left[\mathbf{H}_{gcn,1}^\ell \mid \cdots \mid \mathbf{H}_{gcn,C_{gcn}}^\ell \right]$$

and

$$\mathbf{H}_{sct}^\ell := \left[\mathbf{H}_{sct,1}^\ell \mid \cdots \mid \mathbf{H}_{sct,C_{sct}}^\ell \right],$$

which are the concatenations of channels $\{\mathbf{H}_{gcn,k}^\ell\}_{k=1}^{C_{gcn}}$ and $\{\mathbf{H}_{sct,k}^\ell\}_{k=1}^{C_{sct}}$, respectively. Every $\mathbf{H}_{gcn,k}^\ell$ is defined according to Eq. 2 with the slight modification of added biases and powers of \mathbf{A} , i.e.,

$$\mathbf{H}_{gcn,k}^\ell := \sigma \left(\mathbf{A}^k \mathbf{H}^{\ell-1} \Theta_{gcn,k}^\ell + \mathbf{B}_{gcn,k}^\ell \right).$$

Note that every GCN filter uses a different propagation matrix \mathbf{A}^k and therefore aggregates information from k -step neighborhoods. Similarly, we proceed with $\mathbf{H}_{sct,k}^\ell$ according to Eq. 5 and calculate

$$\mathbf{H}_{sct,k}^\ell := \sigma \left(\Phi_{J_k} \mathbf{H}^{\ell-1} \Theta_{sct,k}^\ell + \mathbf{B}_{sct,k}^\ell \right),$$

where $J_k \in \bigcup_{m \in \mathbb{N}} \mathbb{N}^m$, $k = 1, \dots, C_{sct}$ enables scatterings of different orders and scales. Finally, the GCN components and scattering components get concatenated to

$$\mathbf{H}^\ell := \left[\mathbf{H}_{gcn}^\ell \mid \mathbf{H}_{sct}^\ell \right]. \quad (6)$$

The learned parameters are the weight matrices $\Theta_{gcn,k}^\ell, \Theta_{sct,k}^\ell \in \mathbb{R}^{N_{\ell-1} \times N_\ell}$ coming from the convolutional and scattering layers. These are complemented by vectors of the biases $\mathbf{b}_{gcn,k}^\ell, \mathbf{b}_{sct,k}^\ell \in \mathbb{R}^{N_\ell}$, which are transposed and vertically concatenated n times to the matrices $\mathbf{B}_{gcn,k}, \mathbf{B}_{sct,k} \in \mathbb{R}^{n \times N_\ell}$. To simplify notation, we assume here that all channels use the same number of neurons (N_ℓ). Waiving this assumption would slightly complicate the notation but works perfectly fine in practice.

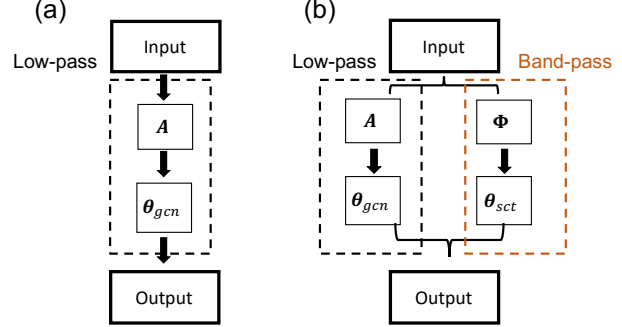


Figure 1. Comparison between GCN and our network: we add band-pass channels to collect different frequency components.

In this work, for simplicity, we limit our architecture to three GCN channels and two scattering channels, as illustrated in Fig. 2. Inspired by the aggregation step in classical geometric scattering, we use $\sigma(\cdot) := |\cdot|^q$ with $q = 4$ as our nonlinearity. However, unlike the powers in Eq. 4, the q -th power here is applied to the node-level instead of moments over the whole graph, retaining the distinction between node-level activations on the graph.

We note that for the first layer, we set the input \mathbf{H}^0 to have the original node features as the graph signal. Each sub-channel (GCN or scattering) transforms the original feature space to a new hidden space with the dimension determined by the number of neurons encoded in the columns of the corresponding submatrix of \mathbf{H}^ℓ . These transformations are learned by the network via the weights and biases. Larger matrices \mathbf{H}^ℓ (i.e., more columns, as the number of nodes in the graph is fixed) indicate the weight matrices have more parameters to learn. Thus, the information in these channels can be propagated well and sufficiently represented.

In general, the width of a channel is relevant to the importance of these regularities. A wider channel suggests these frequency components are more critical and need to be sufficiently learned. Reducing the width of the channel will suppress the magnitude of information that can be learned from a particular frequency window. For more details and analysis of specific design choices in our architecture we refer the reader to Sec. 7, where we discuss them in the context of our experimental results.

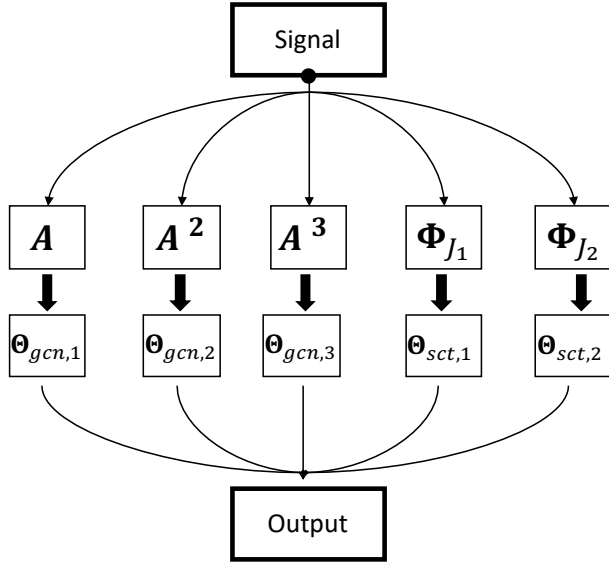


Figure 2. The band-pass layers

6. Graph Residual Convolution

Using the combination of GCN and scattering architectures, we collect multiscale information at the node level. This information is aggregated from different localized neighborhoods, which may exhibit vastly different frequency spectra. This comes for example from varying label rates in different graph substructures. In particular, very sparse graph sections can cause problems when the scattering features actually learn the difference between labeled and unlabeled nodes, creating high-frequency noise. In the classical geometric scattering used for whole-graph representation, geometric moments were used to aggregate the node-based information, serving at the same time as a low-pass filter. As we want to keep the information localized on the node level, we choose a different approach inspired by skip connections in residual neural networks (He et al., 2016). Conceptually, this low-pass filter, which we call *graph residual convolution*, reduces the captured frequency spectrum up to a cutoff frequency as depicted in Fig. 3(b).

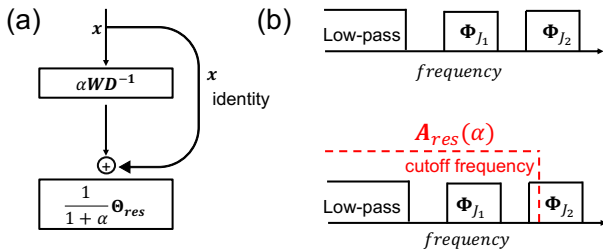


Figure 3. a) The structure of the graph residual convolution layer, b) Schematic depiction in the frequency domain

The graph residual convolution matrix is given by

$$A_{res}(\alpha) = \frac{1}{\alpha + 1}(\mathbf{I}_n + \alpha \mathbf{W} \mathbf{D}^{-1})$$

and we apply it after the hybrid layer of GCN and scattering filters. For $\alpha \rightarrow 0$, we get that $A_{res}(\alpha)$ is the identity (no cutoff) while $\alpha \rightarrow \infty$ results in $\mathbf{R} = \mathbf{W} \mathbf{D}^{-1}$, which can be interpreted as an interpolation between the completely lazy random walk and the non-resting random walk \mathbf{R} .

In our architecture, we apply the graph residual layer on the output H^ℓ of the scattering GCN layer (6). The update rule for this step, illustrated in Fig. 3(a), is then expressed by

$$H^{\ell+1} = A_{res}(\alpha)H^\ell \Theta_{res} + B_{res},$$

where $\Theta_{res} \in \mathbb{R}^{N \times N_{\ell+1}}$ are learned weights, $B_{res} \in \mathbb{R}^{n \times N_{\ell+1}}$ are learned biases (similar to the notations used previously), and N is the number of features of the concatenated layer H^ℓ in Eq. 6. If $H^{\ell+1}$ is the final layer, we choose $N_{\ell+1}$ equal to the number of classes.

7. Results

Compared to shallow GCN models, the proposed hybrid scattering GCN is able to collect a richer range of regularity patterns from the graph. Fig. 4 shows the comparison between Label Propagation (Zhu et al., 2003), GCN used in Kipf & Welling (2016), and GCN with partially absorbing random walks from Li et al. (2018). The oversmoothing caused by the Laplacian kernel and the shallow layers, which limit the collection of information from far-ranging neighbourhoods, restrict the GCN performance when the training size shrinks. The x-axis refers to the proportion of the original training size (1.0 means that we use the original training

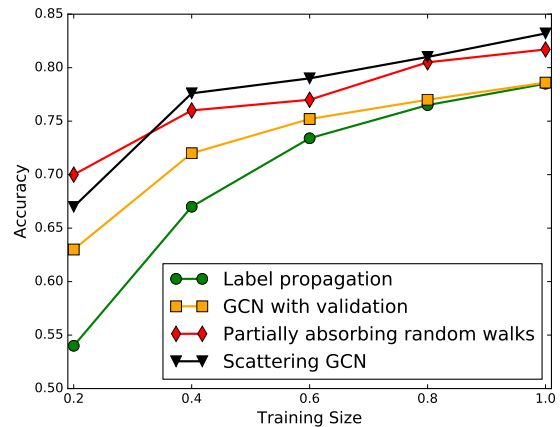


Figure 4. Comparison of different models on the Cora citation network: the x-axis is the ratio of training size compared to the original data split (training/testing: 1000/140) in Kipf & Welling (2016), 0.5 means that the training size reduces to 500 while the testing size stays the same.

Table 1. Dataset statistics

DATASET	NODES	EDGES	FEATURES	LABEL RATE
CITeseer	3,327	4,732	3,703	0.036
CORA	2,708	5,429	1,433	0.052
PUBMED	19,717	44,338	500	0.003

Table 2. Classification accuracies. A: Kipf & Welling (2016), B: Li et al. (2018), C: Veličković et al. (2017), D: Defferrard et al. (2016).

MODEL	CORA	PUBMED	CITeseer
SCATTERING GCN	83.3	79.4	71.0
GCN[A]	81.5	79.0	70.3
PARTIALLY ABSORBING[B]	81.7	79.2	71.2
GAT[C]	83.0	79.0	72.5
CHEBYSHEV[D]	81.2	74.4	69.8

data used in Kipf & Welling (2016), while 0.2 means we use only 20% of the original training data). By preserving more high frequencies and collecting regularity patterns from the entire graph, our scattering GCN outperforms the other methods under small training size conditions.

Compared to the partially absorbing model discussed in Li et al. (2018), it achieves better overall performance, except for extreme conditions when the training size shrinks to 20% of the original data. One explanation for this is that our model may produce high-frequency noise under insufficient labelling conditions, which our simplified architecture cannot filter out sufficiently. During the training, we also notice that shuffling the dataset can result in varying performance.

We evaluate our methods on three datasets summarized in Tab. 1. We train the scattering GCN on Citeseer, Cora and Pubmed, where the nodes are documents and edges are citation links (Sen et al., 2008). The label rate is the number of labelled nodes that are used for training, divided by the total number of nodes in each dataset. A comparison of the classification results on these datasets is presented in Tab. 2.

7.1. Architecture Visualization

In our experiments, the two scattering channels are selected from three first-order scattering and two second-order scattering configurations, including $\Psi_{1,2,3}$, $\Psi_1|\Psi_2$ and $\Psi_2|\Psi_3$. The architectures for different models are shown in Fig. 5. As discussed before, the band-pass filters may cause additional noise in case of insufficiently labelled data. For the Pubmed dataset, we maintain the structure of plain GCN and add narrow band-pass filters. For sufficiently labelled datasets, we expand the width of band-pass filters and enable the model to incorporate more high-frequency information.

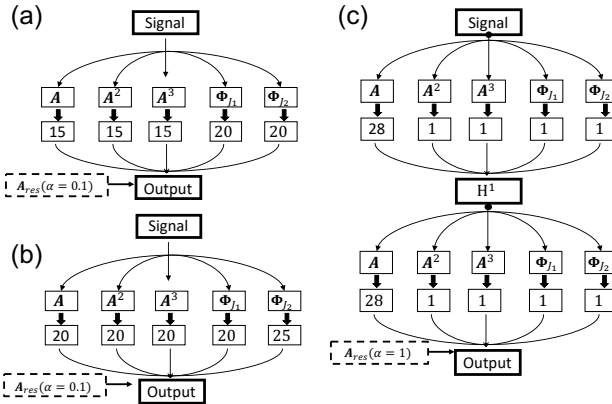


Figure 5. Architecture Visualization. Dataset: a) Cora, b) Citeseer, c) Pubmed. The number indicated under each channel signifies the number of neurons associated with it.

7.2. Parameters

In the following, we provide results from our experiments on the Cora dataset and discuss the choice of parameters. We use L_1 -regularization for every layer and dropout for the first layer. The network structure is shown in Fig. 5(a). We train for a maximum of 200 epochs using Adam (Kingma & Ba, 2014).

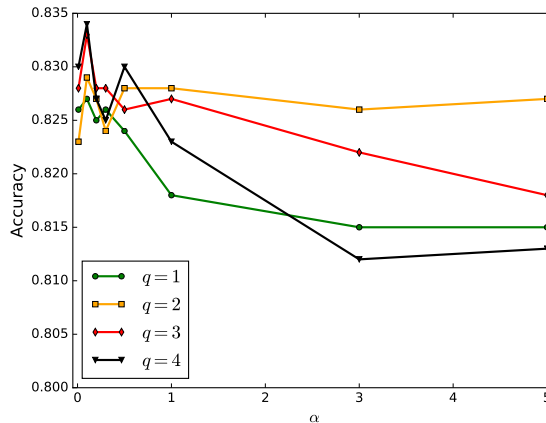


Figure 6. Scattering GCN performance on Cora dataset with different parameters.

To further explore the parameter space, we test our model with different parameters and scattering moments. The results are summarized in Fig. 6. Our experiments suggest that the graph residual convolution plays a critical role in suppressing the high-frequency noise. As shown in Fig. 6, when $\alpha \rightarrow 0$, which is identical to an identity mapping, all frequency components are propagated. As α increases, the performance first increases due to the removal of high-frequency noise. But as α further increases, e.g. when

Table 3. Classification accuracies with $\alpha = 0.1$ with average accuracy 82.9%.

ACCURACY	Ψ_1	Ψ_2	Ψ_3	$\Psi_2 \Psi_3$	$\Psi_1 \Psi_2$
Ψ_1	0.834	0.832	0.833	0.832	0.832
Ψ_2		0.832	0.834	0.828	0.828
Ψ_3			0.828	0.830	0.830
$\Psi_2 \Psi_3$				0.822	0.822
$\Psi_1 \Psi_2$					0.822

Table 4. Classification accuracies with $\alpha = 0.01$ with average accuracy 82.7%.

ACCURACY	Ψ_1	Ψ_2	Ψ_3	$\Psi_2 \Psi_3$	$\Psi_1 \Psi_2$
Ψ_1	0.830	0.829	0.827	0.835	0.835
Ψ_2		0.829	0.831	0.828	0.828
Ψ_3			0.828	0.825	0.825
$\Psi_2 \Psi_3$				0.820	0.820
$\Psi_1 \Psi_2$					0.820

$\alpha = 1$, the layer becomes a random walk model, which stays at the initial location with a probability of one half. This low-pass operation degrades the performance to a level close to Kipf & Welling (2016).

Next, we evaluate the performance of our proposed model with different scattering transformations under different graph residual convolutions. We performed experiments on the graph-based benchmark node classification task on the Cora dataset with different parameters (five different scattering transformations and three different residual convolutions). The results are summarized in Tab. 3, 4 and 5. The rows and columns in these tables denote the two scattering transformation channels used in the scattering GCN, with the structural information shown in Fig. 5 (a).

As shown in Tab. 3, the classification accuracy drops when we use two second-order scattering transformations for the scattering channels. The accuracy is 82.2% for $\Psi_2|\Psi_3$ and $\Psi_1|\Psi_2$. However, we notice that as we replace one second-order scattering transformation by a first-order one, the accuracy increases. This can be attributed to the narrow bandwidth of second-order scattering transformations. As mentioned before, the second-order scattering transformations are less localized in space compared to first-order ones, which suggests that the second-order scattering transformations have wider spatial support. In this case, the frequencies embedded in these channels do not capture the regularity of the graph signal and weaken the performance of the model.

Generally, we limit the models in our experiments to scatterings of a maximal order of two, as higher-order scatterings correspond to a wider spatial support and a narrower frequency band, which are less likely to contain the intrinsic regularity of the graph signal.

We also notice that by combining specific first-order (Ψ_1) and second-order ($\Psi_2|\Psi_3$) scattering transformations and preserving certain high-frequency components ($\alpha = 0.01$),

Table 5. Classification accuracies with $\alpha = 1$ with average accuracy 82.4%.

ACCURACY	Ψ_1	Ψ_2	Ψ_3	$\Psi_2 \Psi_3$	$\Psi_1 \Psi_2$
Ψ_1	0.823	0.820	0.821	0.827	0.827
Ψ_2		0.821	0.823	0.825	0.825
Ψ_3			0.823	0.829	0.829
$\Psi_2 \Psi_3$				0.821	0.821
$\Psi_1 \Psi_2$					0.820

the performance is further increased. This can be interpreted as these filters capturing the critical regularity of the graph signal. However, except for this case, preserving high-frequencies always weakens the network performances in our experiments.

Besides that, we evaluate the performance of our scattering GCN model for different graph residual convolutions. We perform experiments with $\alpha = 0.01$ (close to identity mapping, all frequencies pass), $\alpha = 0.1$ and $\alpha = 1$ (smooth filter). We find that as α increases, the overall performance first increases and then decreases. The average accuracy is 82.7% for $\alpha = 0.01$, 82.9% for $\alpha = 0.1$ and 82.4% for $\alpha = 1$. As discussed before, this suggests that both high frequency noise ($\alpha = 0.01$) and smooth regularity $\alpha = 1$ should be addressed. Thus, the parameter α can be thought of as a 'tradeoff'-parameter in the frequency domain.

8. Conclusion

Our study of semi-supervised node-level classification tasks for graphs shows a new approach for addressing some of the main limitations of GCN models, which are currently the leading (or even state-of-the-art) methods for this task. In this context, we discuss the concept of regularity on graphs and expand the GCN approach, which solely consists in enforcing smoothness, to a richer notion of regularity. This is achieved by incorporating different frequency bands of graph signals, which could not be leveraged in traditional GCN models. We take our inspiration from the concept of geometric scatterings, which have only been used for whole-graph classification so far, and develop a related theory for node-based classification. We also establish the graph residual convolution, drawing inspiration from skip connections in residual networks, which alleviates concerns of high-frequency noise generated in our approach. This results in a toolbox of complementary methods that, combined together, open promising research avenues for advancing semi-supervised learning on graph data, as our experimental results presented in this paper suggest.

Acknowledgements

This work was partially funded by IVADO (l'institut de valorisation des données) and NIH grant R01GM135929.

References

- Abu-El-Haija, S., Perozzi, B., Kapoor, A., Harutyunyan, H., Alipourfard, N., Lerman, K., Steeg, G. V., and Galstyan, A. Mixhop: Higher-order graph convolution architectures via sparsified neighborhood mixing. *arXiv preprint arXiv:1905.00067*, 2019.
- Bronstein, M. M., Bruna, J., LeCun, Y., Szlam, A., and Vandergheynst, P. Geometric deep learning: Going beyond Euclidean data. *IEEE Signal Processing Magazine*, 34(4):18–42, 2017.
- Chung, F. R. K. *Spectral Graph Theory*. American Mathematical Society, 1997.
- Coifman, R. R. and Maggioni, M. Diffusion wavelets. *Applied and Computational Harmonic Analysis*, 21(1):53–94, 2006.
- De Cao, N. and Kipf, T. Molgan: An implicit generative model for small molecular graphs. *arXiv preprint arXiv:1805.11973*, 2018.
- Defferrard, M., Bresson, X., and Vandergheynst, P. Convolutional neural networks on graphs with fast localized spectral filtering. In *Advances in neural information processing systems*, pp. 3844–3852, 2016.
- Fout, A., Byrd, J., Shariat, B., and Ben-Hur, A. Protein interface prediction using graph convolutional networks. In *Advances in neural information processing systems*, pp. 6530–6539, 2017.
- Gama, F., Ribeiro, A., and Bruna, J. Diffusion scattering transforms on graphs, 2018.
- Gama, F., Bruna, J., and Ribeiro, A. Stability of graph scattering transforms, 2019.
- Gao, F., Wolf, G., and Hirn, M. Geometric scattering for graph data analysis. In *International Conference on Machine Learning*, pp. 2122–2131, 2019.
- Gilmer, J., Schoenholz, S. S., Riley, P. F., Vinyals, O., and Dahl, G. E. Neural message passing for quantum chemistry. In *Proceedings of the 34th International Conference on Machine Learning-Volume 70*, pp. 1263–1272. JMLR.org, 2017.
- Hamilton, W., Ying, Z., and Leskovec, J. Inductive representation learning on large graphs. In *Advances in neural information processing systems*, pp. 1024–1034, 2017.
- Hammond, D. K., Vandergheynst, P., and Gribonval, R. Wavelets on graphs via spectral graph theory. *Applied and Computational Harmonic Analysis*, 30(2):129–150, 2011.
- He, K., Zhang, X., Ren, S., and Sun, J. Deep residual learning for image recognition. In *Proceedings of the IEEE conference on computer vision and pattern recognition*, pp. 770–778, 2016.
- Kingma, D. P. and Ba, J. Adam: A method for stochastic optimization. *arXiv preprint arXiv:1412.6980*, 2014.
- Kipf, T. N. and Welling, M. Semi-supervised classification with graph convolutional networks. In *International conference on learning representations*, 2016.
- Knyazev, B., Lin, X., Amer, M. R., and Taylor, G. W. Spectral multigraph networks for discovering and fusing relationships in molecules. *arXiv preprint arXiv:1811.09595*, 2018.
- Li, Q., Han, Z., and Wu, X.-M. Deeper insights into graph convolutional networks for semi-supervised learning. In *Thirty-Second AAAI Conference on Artificial Intelligence*, 2018.
- Liao, R., Zhao, Z., Urtasun, R., and Zemel, R. S. Lanczosnet: Multi-scale deep graph convolutional networks. *arXiv preprint arXiv:1901.01484*, 2019.
- Mallat, S. Group invariant scattering. *Communications on Pure and Applied Mathematics*, 65(10):1331–1398, 2012.
- NT, H. and Maehara, T. Revisiting graph neural networks: All we have is low-pass filters. *arXiv preprint arXiv:1905.09550*, 2019.
- Sen, P., Namata, G., Bilgic, M., Getoor, L., Galligher, B., and Eliassi-Rad, T. Collective classification in network data. *AI magazine*, 29(3):93–93, 2008.
- Shuman, D. I., Ricaud, B., and Vandergheynst, P. Vertex-frequency analysis on graphs, 2013.
- Veličković, P., Cucurull, G., Casanova, A., Romero, A., Lio, P., and Bengio, Y. Graph attention networks. *arXiv preprint arXiv:1710.10903*, 2017.
- Xu, B., Shen, H., Cao, Q., Qiu, Y., and Cheng, X. Graph wavelet neural network. *arXiv preprint arXiv:1904.07785*, 2019.
- Zhu, X., Ghahramani, Z., and Lafferty, J. D. Semi-supervised learning using gaussian fields and harmonic functions. In *Proceedings of the 20th International conference on Machine learning (ICML-03)*, pp. 912–919, 2003.
- Zou, D. and Lerman, G. Graph convolutional neural networks via scattering. *Applied and Computational Harmonic Analysis*, 2019.